

## Preparation of porous Ti35Nb alloy and its mechanical properties under monotonic and cyclic loading

LIN Jian-guo(林建国)<sup>1,2</sup>, ZHANG Yun-fei(张云飞)<sup>1</sup>, MA Mo(马 募)<sup>1</sup>

1. Faculty of Material and Photoelectronic Physics, Xiangtan University, Xiangtan 411105, China;

2. Key Laboratory of Low Dimensional Materials and Application Technology, Ministry of Education, Xiangtan University, Xiangtan 411105, China

Received 14 April 2009; accepted 7 June 2009

**Abstract:** The Ti-35%Nb (mass fraction) foams were prepared by a powder metallurgy method, and the microstructure and the mechanical properties of the foams under monotonic and cyclic loading were investigated. The microstructure of the foams mainly consists of  $\beta$  phase, and the foams exhibit the homogenous pore distribution with the average pore size of 252  $\mu\text{m}$ . The foams with 66% porosity show a typical stress–strain curve of the open-cell foams, and the plateau stress is about 56 MPa. The fatigue strength of the foam is 15.12 MPa at  $10^7$  cycles. The fractographic analysis of the foams reveals that the cracks nucleate within the struts and grow in a fatigue mechanism, resulting in the acceleration of the fatigue damage of the foams.

**Key words:** Ti35Nb foams; fatigue properties; powder metallurgy

### 1 Introduction

Titanium (Ti) and its alloys are frequently used as implant materials in dentistry and orthopedic surgery due to their excellent corrosion resistance, good biocompatibility, high specific strength and relatively low elastic modulus compared with other metallic biomaterials[1–5]. To meet practical requirements of bone ingrowths and long-term implantation, it is necessary to develop new implants that mimic the architecture and low elastic modulus of natural bone, and in the meantime, encourage bone to grow into the pore spaces[6–7]. A scaffold material with a porous structure is a promising implant to meet the above-mentioned requirements and could eliminate the problem of interfacial instability with the host tissue[8–9]. Niobium (Nb), acting as a  $\beta$ -phase stabilizing element and a biocompatible element, has attracted much attention to take great deal of efforts on it and it has been added to many  $\beta$ -Ti alloys and near  $\beta$ -Ti alloys. The Ti-35%Nb (mass fraction) (Ti35Nb) alloy shows good shape memory effects because of the presence of the  $\alpha''$  phase[10]. But, when the alloy is used as biomaterials, the stress-shielding effects caused by the elastic modulus

mismatching between the alloy and canceller bones must be paid attention. One of the effective methods to decrease the elastic modulus of Ti35Nb is to make it a porous material. Thus, in the present work, the porous Ti35Nb alloy was fabricated by a powder metallurgy method and at the same time the mechanical properties of the porous alloy, including the compression and fatigue behavior, were reported.

### 2 Experimental

Elemental powders of titanium (purity 99.9%, size  $\leq 45 \mu\text{m}$ ) and niobium (purity 99.8%, size  $\leq 45 \mu\text{m}$ ) were mixed in the targeted composition of Ti35Nb (mass fraction, %). The mixture was ball-milled at room temperature for 2 h in a planetary ball mill (Retsch PM 400) with stainless steel containers and balls. The ball to powder mass ratio and rotation speed in milling were maintained at 20:1 and 200 r/min, respectively.

The ball-milled powders were mixed with the ammonium bicarbonate particles with the size in the range of 300–500  $\mu\text{m}$  as space holders and then compacted into cylindrical bars under a pressure of 750 MPa. The green compacts were sintered in a vacuum furnace under a pressure of about 1 kPa. The sintered

condition was 175 °C, 4 h + 1 200 °C, 2 h. Finally, the open-cell Ti35Nb foams with different porosities were obtained. The detailed description of the preparation and characteristic of the foam of TiZr can be found in the previous literature[11]. The microstructure of the sintered foams was investigated using scanning electron microscopy (SEM) and X-ray diffraction (XRD) measurements were carried out in order to verify the phase constitution of the compacts after being sintered at 1 200 °C for 2 h.

Compressive tests were performed at room temperature by using a RG2000 test machine with a strain rate of  $10^{-3} \text{ s}^{-1}$ . The dimension of the tested samples was 5.0 mm × 5.0 mm × 10.2 mm. Compression–compression fatigue tests were performed on a servohydraulic test machine (CSS-280S-20) and the dimension of the tested sample in fatigue test was  $d$  9.4 mm × 14.6 mm. The load was applied as a sinus wave function with a frequency of 10 Hz. To generate endurance limit–cycling number curves, the maximum load for successive tests was decreased at 5% intervals until samples survived for  $10^7$  cycles. The applied stress levels were normalized by the corresponding plateau strength of specimen, i.e.  $|\sigma|_{\max}/\sigma_{\text{pl}}$ . The fracture surfaces of the porous alloy were examined by SEM.

### 3 Results and discussion

#### 3.1 Microstructure of porous Ti35Nb specimens

Fig.1 shows the XRD pattern of Ti35Nb foam with a porosity of 66%. The diffraction peaks on the XRD patterns mainly come from  $\beta$ -Ti phase, but some weak peaks of  $\text{Ti}_3\text{O}$  can still be observed. This implies that the sintered sample primarily consists of  $\beta$ -Ti phase, but ball milling introduces oxygen into the powders, resulting in the formation of Ti oxides, as indicated by the XRD patterns.

The typical SEM micrograph of the Ti35Nb foam

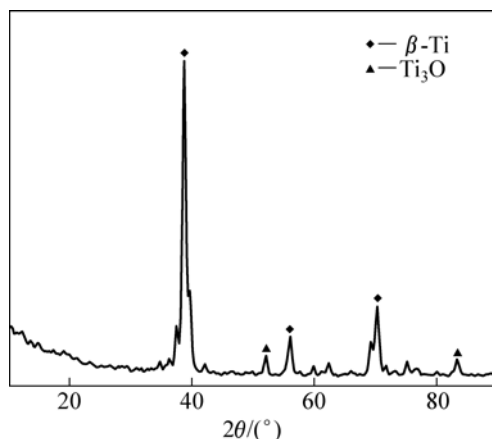


**Fig.1** XRD pattern of Ti35Nb foam sintered at 1 200 °C for 2 h

(porosity of about 66%) on transversal sections is shown in Fig.2. The quantitative image analysis results indicate that the average pore size on the transversal section is 252  $\mu\text{m}$ . The porous sample contains two types of pores, i.e., small isolated micropores distributing in the cell wall of the open interconnected macropores induced by the volume shrinkages during the sintering process of the powders, and interconnective macropores created by the space holders, as shown in Fig.2. The cell walls of the macropores of the porous metals are relatively rough and honeycomb-like. These features of microporous and rugged wall-surface of macropores are preferable in the osteoinductivity[12].

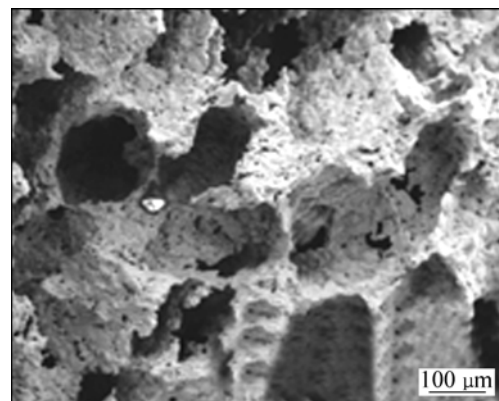


**Fig.2** Typical SEM micrograph of Ti35Nb foams

#### 3.2 Compressive properties

The nominal stress—nominal strain curves of the porous samples with different porosities are shown in Fig.3 and they are composed of three stages. The first stage is the elastic phase, in which cell walls are compressed elastically; the second stage is a plateau region, in which the specimens deform under a constant flow stress (plateau stress); and the third stage is the densified phase, in which all of the pores are completely destroyed and the porous sample is densified, leading to

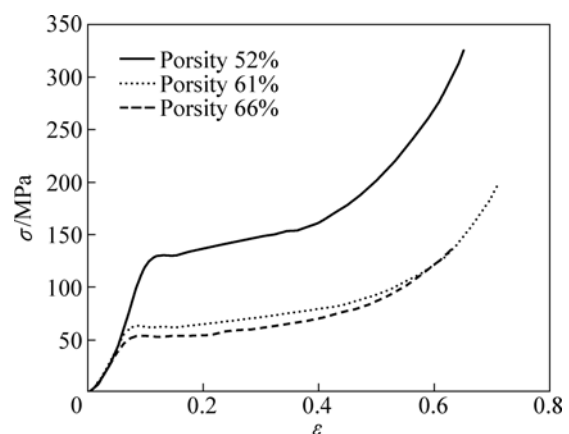


**Fig.3** Nominal stress—nominal strain curves of Ti35Nb specimens with different porosities

the stress increasing dramatically. The plateau stresses and the elastic modulus of the three samples obtained from stress–strain curves are presented in Fig.4. It is apparent that the plateau stress and elastic modulus are strongly dependant on the porosity of the samples. With the increase of the porosity, both of them decrease significantly. Compared with the mechanical properties of the nature bones in Table 1, those of the porous alloy with the porosities ranging from 52% to 66% lie in the range of nature bones. This should be borne in mind with regard to minimize the stress shielding effects in load transfer from implant to bone and suggests that the Ti35Nb foams could be used as a new kind of biomaterials in the near future.

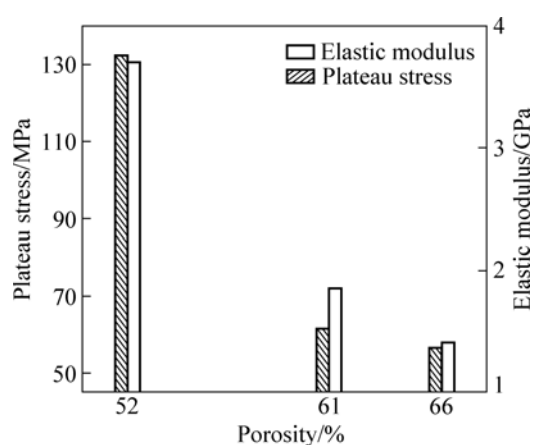


**Fig.4** Plateau strength and elastic modulus of porous Ti35Nb alloy as function of porosity

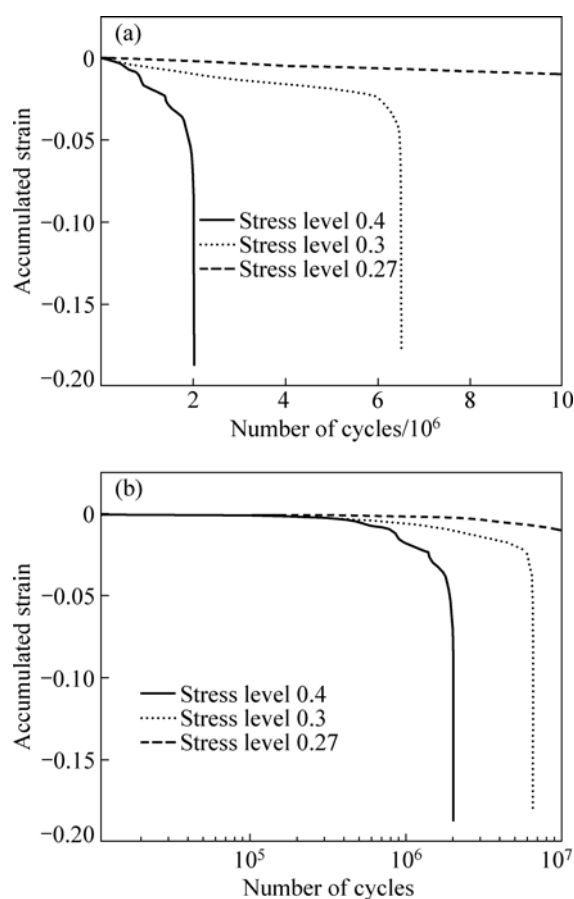
**Table 1** Mechanical properties of porous Ti35Nb alloy in comparison with natural bones

Material	Porosity/%	Plateau strength/MPa	Elastic modulus/GPa	Reference
Porous Ti35Nb alloy	52	131	3.7	This work
	61	60	1.8	
	66	56	1.3	
Natural bone	–	2–180	0.1–20	[13–15]

### 3.3 Fatigue behavior

During the fatigue tests, the cyclic strain accumulation leads to the progressive shortening of the specimens. The curves of the accumulated strain versus the number of fatigue cycles under different stress levels are presented in Fig.5. To clarify the strain accumulation process, a linear scale and a half logarithmic scale were used in Fig.5(a) and Fig.5(b), respectively. It can be seen that the strain accumulation may be classified into three stages, according to the shortening rate. In the first stage, a small strain of 0.002–0.003 accumulates at the very beginning of cyclic loading, and the strain remains almost unchanged or is slightly increased. Then, the

strain accumulation enters into the second stage, in which the strain accumulates to 0.015–0.04 according to different stress levels in a short duration. The third stage starts immediately after the second stage, and a sharply rapid strain accumulation or the so-called strain jump occurs, and the specimens are severely shortened. These characteristics are in agreement with those of Al foams reported in previous studies[16–17].



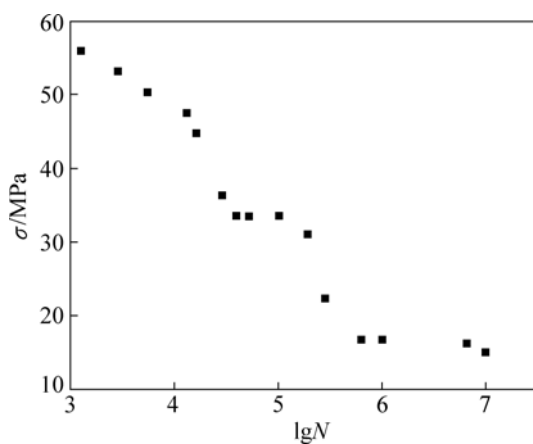
**Fig.5** Plots of accumulated strain vs number of cycles for specimens tested at different stress levels: (a) With linear scale; (b) With half logarithmic scale

Fig.6 presents the endurance limit—cycling number curves of the porous sample with a porosity of 66%. The endurance limit is also defined as the highest stress level, at which the tested specimens survive for  $10^7$  cycles under fatigue loading. These definitions are consistent with those used by other authors[16–17]. It can be seen that with the decrease of stress level, the serving time is sharply increased. When the sample was tested at the stress level of 0.27 (15.12 MPa), the porous sample does not show any breakage after  $10^7$  cycles. Therefore, this means that the fatigue strength of Ti35Nb foams is about 15.12 MPa.

Figs.7(a) and (b) present the typical fatigue fracture surface of the porous sample after  $10^5$  cycles tested at stress level of 0.3. Cells in the interior of the specimen

are visible. A crack initiates at a micropore on the cell wall, indicated by the arrow in Fig.7(b). The crack crosses the thin cell and makes the strut broken, as seen in Fig.7(a). During the fatigue test, the struts and cell walls of the porous specimens support cyclic loadings. Cracks are easily triggered around the micropores because of a high stress concentration at this position. Under the cyclic loading condition, the cracks propagate to a critical size, which causes the strut to break. Once the strut failed, the loads are transferred to adjacent cell walls, leading to the acceleration of the failure of the adjacent cell walls.

Close observation under SEM shows that the fatigue



**Fig.6** Endurance limit—cycling number curves of Ti35Nb metallic foams

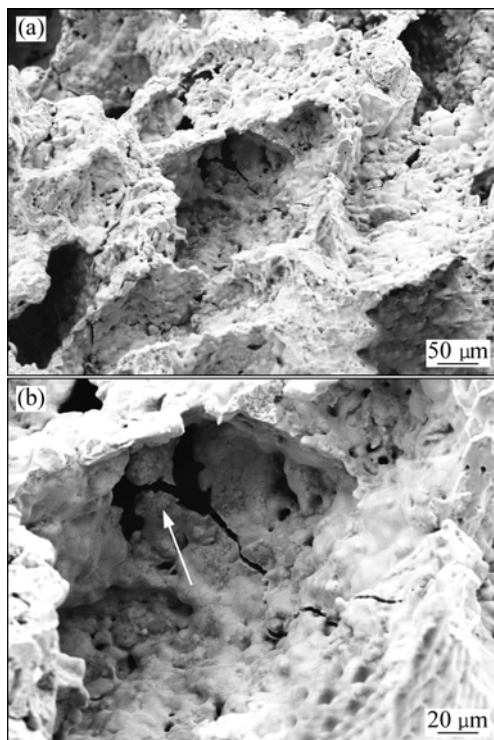


**Fig.7** Cracks in cell walls of specimen tested at stress level of 0.3: (a) Cracks within cell walls; (b) Cracks in higher magnification indicated by arrow

fracture surface is relatively smooth and composed of transcrystallines, as seen in Fig.8(a). Some striations can be observed in some areas, as shown in Fig.8(b). The fatigue striations are different from those in solid samples under the cyclic compression loadings, implying that the fatigue fracture of the cell wall is in a combination of the fracture modes under the complicated stresses. By carefully studying the fatigue fractography of the specimens (as seen in Fig.8(a)), we can deduce the process of the fatigue crack propagation. The fatigue crack propagation rate is very low in the early stage. After a long serving time, the fatigue crack propagates steadily, which is indicated by the fatigue striations in the region marked with A. When the crack propagates to a critical size, an instantaneous breaking occurs in a cleavage cracking mode or faceted and flat cracking mode in the regions marked with B and C. Therefore, it can be concluded that the crack meandering propagates from region A to region B and C and the strut is broken instantaneously in region C. The results of the fractography analysis are in agreement with the strain accumulation rates with the cycle number.

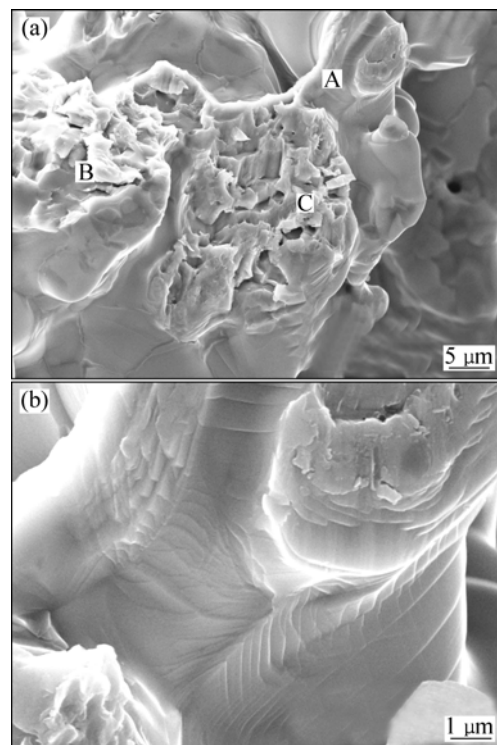


**Fig.8** Fracture surface morphologies of specimen after breaking fatigue crack propagation and instantaneous fracture regions (a), and striations under high magnification on strut (b)

## 4 Conclusions

- 1) The porous alloy exhibits a homogenous pore structure with an average pore size of 252 μm.
- 2) The plateau stress and elastic modulus of the porous alloy are strongly dependant on their porosity.

With the increase of the porosity from 52% to 66%, the plateau stress and elastic modulus decrease from 131 MPa to 56 MPa and from 3.7 GPa to 1.3 GPa respectively.

3) The fatigue strength of the porous alloy is about 15.12 MPa after  $10^7$  cycles. The fatigue cracks preferentially initiate at the positions of micropores and propagate along the thin cell walls by a fatigue mechanism. Once the strut failed, the loads are transferred to the adjacent struts, leading to the acceleration of the failure of the porous alloys.

## Acknowledgements

The authors also wish to thank the help of Dr. JIANG Yong in College of Civil Engineering and Mechanics of Xiangtan University, China.

## References

- [1] BANHART J. Manufacture, characterisation and application of cellular metals and metal foams [J]. *Progress in Materials Science*, 2001, 46: 559–632.
- [2] ASHBY M F, EVANS A, FLECK N A, GIBSON L J, HUTCHINSON J W, WADLEY H N G. *Metal foams—A design guide* [M]. Woburn, MA: Butterworth-Heinemann, 2000.
- [3] SIMSKE S J, AYERS R A, BATEMAN T A. Porous materials for bone engineering [J]. *Materials Science Forum*, 1997, 250: 151–182.
- [4] MITSUO N. Fatigue performance and cyto-toxicity of low rigidity titanium alloy, Ti-29Nb-13Ta-4.6Zr [J]. *Biomaterials*, 2003, 24: 2673–2683.
- [5] OKAZAKI Y, SETHUMADHAVAN R, TATEISHI T, YOSHIMASA I. Cytocompatibility of various metal and development of new titanium alloys for medical implants [J]. *Materials Science and Engineering A*, 1998, 243: 250–256.
- [6] FREYMAN T M, YANNAS I V, GIBSON L J. Cellular materials as porous scaffolds for tissue engineering [J]. *Progress in Materials Science*, 2001, 46: 273–282.
- [7] GOMES M E, RIBEIRO A S, MALAFAYA P B, REIS R L, CUNHA A M. A new approach based on injection moulding to produce biodegradable starch-based polymeric scaffolds: Morphology, mechanical and degradation behaviour [J]. *Biomaterials*, 2001, 22: 883–889.
- [8] WEN C E, YAMADA Y, SHIMOJIMA K, CHINO Y, HOSOKAWA H, MABUCHI M. Novel titanium foam for bone tissue engineering [J]. *Journal of Materials Research*, 2002, 10: 2633–2639.
- [9] WEN C E, YAMADA Y, SHIMOJIMA K, CHINO Y, HOSOKAWA H, MABUCHI M. Compressibility of porous magnesium foam: Dependency on porosity and pore size [J]. *Materials Letter*, 2004, 58: 357–360.
- [10] BAKER C. The shape memory effect in a titanium-35wt% niobium alloy [J]. *Metal Science Journal*, 1971, 5: 92–100.
- [11] WEN C E, YAMADA Y, HONGSON P D. Fabrication of novel TiZr alloy foams for biomedical applications [J]. *Materials Science and Engineering C*, 2006, 26: 1439–1444.
- [12] BARRABES M, SEVILLA P, PLANEL J A I, GIL F J. Mechanical properties of nickel-titanium foams for reconstructive orthopaedics [J]. *Materials Science and Engineering C*, 2008, 28: 23–27.
- [13] STAIGER M P, PIETAKA A M, HUADNMAIA J, DIAS G. Magnesium and its alloys as orthopedic biomaterials: A review [J]. *Biomaterials*, 2006, 27: 1728–1734.
- [14] KARAGEORGIOU V, KAPLAN D. Porosity of 3D biomaterial scaffolds and osteogenesis [J]. *Biomaterials*, 2005, 26: 5474–5491.
- [15] REZWAN K, CHEN Q Z, BLAKER J J, BOCCACCINI A R. Biodegradable and bioactive porous polymer/inorganic composite scaffolds for bone tissue engineering [J]. *Biomaterials*, 2006, 27: 3413–3431.
- [16] ZHOU J, SOBOYEJO W O. Compression-compression fatigue of open cell aluminum foams: macro-/micro-mechanisms and the effects of heat treatment [J]. *Materials Science and Engineering A*, 2004, 369: 23–35.
- [17] HARTE A M, FLECK N A, ASHBY M F. Fatigue failure of an open cell and a closed cell aluminum alloy foam [J]. *Acta Mater*, 1999, 47: 2511–2524.

(Edited by YANG Bing)